Adipose-Derived Mesenchymal Stem Cells Prevent Systemic Bone Loss in Collagen-Induced Arthritis

Manasa G. Garimella,* Supinder Kour,* Vikrant Piprode,* Monika Mittal,† Anil Kumar,* Lekha Rani,* Satish T. Pote,* Gyan C. Mishra,* Naibedya Chattopadhyay,† and Mohan R. Wani*

Rheumatoid arthritis (RA) is an autoimmune disease characterized by chronic inflammatory synovitis leading to joint destruction and systemic bone loss. The inflammation-induced bone loss is mediated by increased osteoclast formation and function. Current antirheumatic therapies primarily target suppression of inflammatory cascade with limited or no success in controlling progression of bone destruction. Mesenchymal stem cells (MSCs) by virtue of their tissue repair and immunomodulatory properties have shown promising results in various autoimmune and degenerative diseases. However, the role of MSCs in prevention of bone destruction in RA is not yet understood. In this study, we investigated the effect of adipose-derived MSCs (ASCs) on in vitro formation of bone-resorbing osteoclasts and pathological bone loss in the mouse collagen-induced arthritis (CIA) model of RA. We observed that ASCs significantly inhibited receptor activator of NF-κB ligand (RANKL)–induced osteoclastogenesis in both a contact-dependent and -independent manner. Additionally, ASCs inhibited RANKL-induced osteoclastogenesis in the presence of proinflammatory cytokines such as TNF-α, IL-17, and IL-1β. Furthermore, treatment with ASCs at the onset of CIA significantly reduced clinical symptoms and joint pathology. Interestingly, ASCs protected periarticular and systemic bone loss in CIA mice by maintaining trabecular bone structure. We further observed that treatment with ASCs reduced osteoclast precursors in bone marrow, resulting in decreased osteoclastogenesis. Moreover, ASCs suppressed autoimmune T cell responses and increased the percentages of peripheral regulatory T and B cells. Thus, we provide strong evidence that ASCs ameliorate inflammation-induced systemic bone loss in CIA mice by reducing osteoclast precursors and promoting immune tolerance. ***The Journal of Immunology*****, 2015, 195: 5136–5148.**

Human rheumatoid arthritis (RA) is an autoimmune disease characterized by chronic inflammatory synovitis and production of autoantibodies and several proinflammatory cytokines, which together lead to joint destruction (1). Inflammation-induced bone destruction is a key pathological feature of RA, mediated by osteoclasts. Osteoclasts are formed by the fusion of myeloid precursors of monocyte/macrophage lineage in the presence of receptor activator of NF-κB ligand (RANKL) and M-CSF (2). The proinflammatory milieu of the arthritic synovium leads to aberrant differentiation and activation of osteoclasts, resulting in massive bone loss (3). Chronic inflammation also shifts the equilibrium of bone remodeling toward increased bone resorption rather than formation, leading subsequently to systemic osteopenia associated with an enhanced risk for osteoporotic fractures (4). Current antirheumatic therapies primarily target the suppression of inflammatory cascade with varying success in limiting the progression of bone destruction (5). Therefore, better therapeutic agents are needed affecting both inflammatory processes and skeletal damage.

Mesenchymal stem cells (MSCs) are adult multipotent nonhematopoietic stem cells of mesodermal origin that can differentiate into cells of both mesenchymal and nonmesenchymal lineages (6, 7). Initially identified from bone marrow, MSCs have been isolated from various sources, including adipose tissue, gingiva, umbilical cord, and many other adult tissues (8). In addition to their regenerative potential, they exert profound immunomodulation by affecting proliferation, differentiation, and maturation of various immune cell types (9). MSCs are also known to home to the site of injury or inflammation and contribute to tissue repair processes locally through trophic factors (10). Because of the unique combination of these properties, MSCs are being widely studied in clinical trials of various autoimmune disorders and degenerative diseases (11, 12).

Despite several conflicting reports, MSCs from various tissues have shown protective effect in reducing autoimmune and inflammatory processes in preclinical models of RA (13–15). However, the role of MSCs in protecting skeletal component of arthritis, including pathological bone loss and the bone-resorbing osteoclasts, has not been well studied. Also, earlier studies on the role of MSCs

*National Centre for Cell Science, Ganeshkhind, Pune 411 007, India; and †Division of Endocrinology, Council of Scientific and Industrial Research–Central Drug Research Institute, Lucknow 226 031, India

Received for publication February 10, 2015. Accepted for publication September 30, 2015.

This work was supported by Department of Biotechnology, India Grant BT/HRD/34/01/2009 (to M.R.W.), as well as Council of Scientific and Industrial Research, New Delhi, India Grant BSC0201 (to N.C.). M.G.G. is the recipient of a senior research fellowship from the Council for Scientific and Industrial Research, New Delhi, India.

Address correspondence and reprint requests to Dr. Mohan R. Wani, National Centre for Cell Science, Savitribai Phule Pune University Campus, Ganeshkhind Road, Pune 411 007, India. E-mail address: mohanwani@nccs.res.in

The online version of this article contains supplemental material.

Abbreviations used in this article: ASC, adipose-derived mesenchymal stem cell; BMD, bone mineral density; Breg, regulatory B cell; BV/TV, trabecular bone volume fraction; CFU-F, CFU-fibroblast; CIA, collagen-induced arthritis; CII, collagen type II; CM, conditioned medium; Conn. D, connectivity density; Cs. Th, cross-sectional thickness; μCT, microcomputed tomography; Ct. BMD, cortical BMD; CTR, calcitonin receptor; DC-STAMP, dendritic cell–specific transmembrane protein; dLN, draining lymph node; MMP, matrix metalloproteinase; MNC, multinuclear cell; MSC, mesenchymal stem cell; OCP, osteoclast precursor; RA, rheumatoid arthritis; RANK, receptor activator of NF-κB; RANKL, receptor activator of NF-κB ligand; rm, recombinant murine; Tb. BMD, trabecular BMD; Tb. N, trabecular number; Tb. Sp, trabecular separation; Tb. Th, trabecular thickness; TRAP, tartrate-resistant acid phosphatase; Treg, regulatory T cell.

in osteoclast differentiation are conflicting, with both stimulatory (16, 17) as well as inhibitory (18, 19) effects. Therefore, in the present study, we investigated the effect of MSCs on the differentiation of bone-resorbing osteoclasts and inflammation-induced bone loss in the mouse collagen-induced arthritis (CIA) model. We used syngeneic adipose-derived MSCs (ASCs) for our study because of their ease of isolation and relative abundance.

In this study, we found that ASCs inhibited RANKL-induced osteoclast differentiation in vitro in both a contact-dependent and -independent manner. ASCs protected against disease severity and bone loss in CIA mice as evaluated by histomorphometric measurements of trabecular bone indices. Decreased bone loss was found to be a result of decreased osteoclast precursors (OCPs) in bone marrow and increased peripheral regulatory T cell (Treg) and B cell (Breg) percentages. This study clearly suggests that ASCs exert a strong therapeutic effect in RA by preventing bone loss along with dampening the ongoing inflammatory responses.

Materials and Methods

Animals

Male and female DBA/1J (6–12 wk old) mice were obtained from the Experimental Animal Facility of the National Centre for Cell Science, Pune, India. Water and food were provided ad libitum. All experiments involving animal use were approved by the Institutional Animal Ethics Committee.

Abs and reagents

The following Abs were purchased from BD Biosciences: purified anti-CD3ε (145-2C11, NA/LE), purified anti-CD28 (37.51, NA/LE), Pacific Blue (PB)–anti-CD4 (RM4-5), allophycocyanin–anti-Foxp3 (FJK-16s), PE–anti-CD19 (1D3), Alexa Fluor 488–anti-c-fms (AFS98), PE-Cy7–anti-CD11b (M1/70), allophycocyanin–anti-CD11c (HL3), allophycocyanin–anti-F4/80 (BM8), PE–anti-RANK (R12-31), PE–anti-c-Kit (2B8), PE–anti-B220 (RA3-6B2), PerCP-Cy5.5–anti-CD1d (1B1), PE-Cy7–anti-CD5 (53-7.3), PE–anti-CD105 (MJ7/18), allophycocyanin–CD29 (HMβ1-1), FITC–anti-CD44 (IM7), FITC–anti-Sca-1 (D7), FITC–anti-MHC class II, PE–anti-CD90 (53-2.1), FITC–anti-CD34 (RAM34), FITC–anti-CD14 (rmC5-3), allophycocyanin–anti-platelet-derived growth factor receptor (APA5), PE–anti-H-2D^d (34-5-8S), PE–rat IgG2ak, PerCP-Cy5.5–rat IgG2bk, PE–rat IgG2bk, PE–Cy7-rat IgG2bk, allophycocyanin–rat IgG2ak, Alexa Fluor 488–rat IgG2ak, Pacific Blue–rat IgG2bk, allophycocyanin–armenian hamster IgG1λ2, PE-Cy7–rat IgG2b,k, PE-Cy7–rat IgG2ak, PE-Cy7–rat IgG1, allophycocyanin–armenian hamster IgG, FITC–rat IgG2bk, FITC–rat IgG2ak, FITC–rat IgG1k, PE–mouse IgG2ak. PE-Cy7–anti-CD73 (TY/11.8) and PE–anti-IL-17A (eBio17B7) were from eBioscience.

Foxp3 staining buffer and RBC lysis buffer were from eBioscience. Mouse T cell activation Dynabeads were obtained from Life Technologies. PMA and ionomycin, dexamethasone, β-glycerophosphate, ascorbic acid, naphthol AS-BI phosphate, sodium tartarate, native chicken sternal collagen type II (CII), and IFA were purchased from Sigma-Aldrich. CFA was from Chondrex. Recombinant human M-CSF, recombinant murine (rm) TNF-α, rmIL-17, rmIL-6. and rmIL-1β were obtained from R&D Systems. Soluble rmRANKL was from PeproTech. Adipogenic and chondrogenic induction kits were obtained from Lonza. All cultures were maintained at 37°C in a humidified atmosphere of 5% CO_2 in air.

Isolation of ASCs

Murine ASCs were isolated as described by Sung et al. (20) with slight modifications. Subcutaneous adipose tissue isolated from 10- to 12-wk-old DBA/1J mice was digested with 2 mg/ml collagenase (type 1A, Sigma-Aldrich) in PBS at 37°C for 15–20 min. The cell suspension obtained after filtration through 40-nm nylon filter mesh (BD Falcon) was centrifuged and then seeded at a density of 5×10^4 cells/ml and cultured in DMEM (containing 4.5 g/l glucose) supplemented with 10% FCS, 100 U/ml penicillin, 100 μg/ml streptomycin, and 2 mM L-glutamine. Nonadherent cells were discarded after 72 h and adherent cells were maintained until they attained 80–90% confluency. Cells were passaged using trypsin-EDTA and split in a ratio of 1:3.

CFU-fibroblast assay

To assess the clonogenic potential of ASCs, a CFU-fibroblast (CFU-F) assay was performed as described previously (21). Briefly, 1×10^3 cells were cultured in a 60-mm petri dish for 7–10 d followed by formalin fixation and staining with hematoxylin. Cultures were observed for colonies with aggregates of 50 or more cells using a bright-field microscope and were scored as CFU-F.

In vitro osteogenic, adipogenic, and chondrogenic differentiation of ASCs

Induction of osteoblast, adipocyte, and chondrocyte differentiation was performed as described previously (21). For osteoblast differentiation, monolayer cultures of mouse ASCs ($2–5 \times 10^3$ cells/cm^2) were incubated in α-MEM containing 10% FCS, 10 mM β-glycerophosphate, 50 μg/ml ascorbic acid, and 100 nM dexamethasone for 21–25 d. Cultures were half fed every third day and assessed for matrix mineralization by Alizarin red S staining. For Alizarin red S staining, cells were washed with PBS, fixed in 10% formalin, and incubated with 2% Alizarin red S for 2 min at room temperature. Cells were washed with distilled water and observed for mineralization as red calcium deposits. Alizarin red S was eluted in 10% glacial acetic acid and quantitated colorimetrically at 405 nm.

For adipogenic differentiation, ASCs ($2–5 \times 10^3$ cells/cm^2) were incubated until they attained 90% confluency. Adipogenesis was induced using a commercial kit from Lonza. Briefly, cells were incubated in adipogenic induction medium (DMEM with 4.5 g/l glucose, 10% FCS, 1 μM dexamethasone, 10 μM insulin, 0.5 mM 3-isobutyl-1-methylxanthine, and 100 nM indomethacin) for 3 d, followed by 1 d in maintenance medium (DMEM with 4.5 g/l glucose, 10% FCS, and 10 μM insulin) constituting one cycle of induction and maintenance. After multiple rounds of induction and maintenance for 25–30 d, cells were examined for formation of oil globules by Oil Red O staining. Cells were formalin fixed, stained with Oil Red O (3 mg/ml) for 1 h at room temperature, and were observed under a bright-field microscope for the formation of oil globules.

For chondrogenic differentiation, 2×10^5 ASCs were pelleted down in round-bottom 96-well plates to form a pelleted micromass at the bottom of the well. Pellets were incubated in serum-free DMEM (4.5 g/l glucose) containing 0.1 μM dexamethasone, 50 μg/ml ascorbic acid, 1 mM sodium pyruvate, 40 μg/ml L-proline, 6.25 μg/ml ITS, and 10 ng/ml TGF-β3. After 21 d, cell pellets were fixed in 10% formalin, and 5-μm sections were stained with H&E to evaluate histology.

Preparation of conditioned medium from ASCs

ASC-conditioned medium (ASC-CM) was prepared by culturing ASCs of passages 2 or 3 at 70–90% confluency in α-MEM supplemented with 10% FCS for 24 h. Culture supernatant was collected, centrifuged, and stored at −80°C until use.

Induction of CIA

Native CII was dissolved in 50 mM acetic acid at 4°C overnight and emulsified with an equal volume of CFA (containing 4 mg/ml *Mycobacterium tuberculosis*; strain H37Ra). DBA/1J mice (8–10 wk old) were injected with 100 μl emulsion containing 200 μg CII intradermally at the base of the tail. At day 21 after primary immunization, mice were given a booster with 200 μg CII emulsified in an equal volume of IFA, through the same route, and randomly divided into two groups. On day 22, 2×10^6 murine syngeneic ASCs in 100 μl PBS per mouse were administered i.p. to one group (CIA plus ASCs) and an equal volume of PBS was administered to the other group (CIA plus PBS). Mice were monitored for signs of arthritis by two blinded observers using two clinical parameters: paw swelling and arthritic score. Paw swelling was evaluated by measuring thickness of affected hindpaws using 0–10 mm calipers. Clinical arthritis was assessed by the following scoring system: 0, no evidence of erythema and swelling; 1, erythema and mild swelling limited to tarsals or ankle joint; 2, erythema and mild swelling extending from ankle to tarsal joints; 3, erythema and moderate swelling extending from ankle to metatarsal joints; 4, erythema and severe swelling surrounding the ankle, foot, and digits. Each limb was graded individually, giving a maximum possible score of 16 per animal. Hindlimbs were evaluated by soft x-ray radiography (Siemens). Mice were sacrificed on day 36 and studied for various disease parameters.

Histology

For histological analysis, whole knee joints were excised and fixed in 10% formalin for 4 d. Decalcification was done in 5% formic acid and the specimens were processed for paraffin embedding. Next, 5-μm sections were prepared and stained with H&E.

Measurement of serum anti-CII Abs

Peripheral blood was collected from mice by orbital sinus puncture and sera were obtained using BD vaccutainer tubes. Sera were then tested for anti-CII

Abs by ELISA using a commercial kit (Chondrex) following the manufacturer's instructions.

T cell proliferation assay

Single-cell suspensions were prepared from draining lymph nodes (dLNs) and cultured in 96-well plates (5×10^5 cells/well) in presence of CII (40 μg/ml) or plate-bound anti-CD3ε (2 μg/ml) for 72 h. Cells were pulsed with [^{3}H]thymidine (1 μCi/well) during the last 18 h of the culture period and harvested using a 96-well cell harvester (PerkinElmer). Incorporated radioactivity was measured as cpm, using a beta liquid scintillation counter (Packard). For in vitro coculture assays of ASCs and T cells, CD4$^+$ T cells were isolated from spleens of normal mice using CD4$^+$ T cell enrichment mixture (BD Biosciences) by magnetic selection. Stimulation index was calculated by the formula: cpm in response to Ag/cpm in absence of Ag.

Flow cytometric analysis

Single-cell suspensions prepared from peritoneum, synovium, peripheral blood, spleen, and dLNs were stained with Pacific Blue–anti-CD4 Ab for 30 min. Cells were washed thoroughly with stain buffer (Dulbecco's PBS plus 2% FCS) and fixed/permeabilized with Foxp3 permeabilization buffer for 60 min. Intracellular staining was performed using allophycocyanin-conjugated anti-Foxp3 Ab in permeabilization buffer for 45 min. Cells were washed with permeabilization buffer and analyzed by flow cytometry.

For surface staining, single-cell suspensions of ASCs, splenocytes, or bone marrow cells were fixed with 4% paraformaldehyde for 10 min at room temperature and washed with stain buffer. Then, 1×10^5–10^6 cells per tube were stained with fluorochrome-conjugated Abs for 45 min on ice, along with appropriate isotype controls in separate tubes. Cells were washed with stain buffer twice and acquired on a FACSCanto II (BD Biosciences). All steps were performed in dark at 4°C. Data were analyzed using FlowJo (Tree Star) software.

For Tregs, lymphocytes based on forward scatter and sides scatter were gated and measured for percentages of CD4 and Foxp3 dual-positive populations. For Bregs, a lymphocyte cluster was gated for the CD19$^+$ population and measured for CD1d^{hi} and CD5$^+$ populations. All gates were set based on isotype controls.

Osteoclastogenesis and tartrate-resistant acid phosphatase measurement

Murine osteoclasts were generated as described previously (22). Briefly, bone marrow cells from mice were cultured overnight with 7 ng/ml recombinant human M-CSF. Nonadherent cells were harvested, RBC lysed, and cultured in the presence of M-CSF (30 ng/ml) and varying concentrations of soluble RANKL for 3–4 d. Tartrate-resistant acid phosphatase (TRAP) staining was then performed in presence of 0.05 M sodium tartrate using napthol AS-BI phosphate as substrate. TRAP$^+$ cells with three or more nuclei were counted as osteoclasts.

Pit formation assay

Osteoclasts were differentiated as mentioned above in 96-well plates coated with a thin film of calcium phosphate (Osteo assay plates, Nunc) for 8 d. Cells were bleached with 4% sodium hypochlorite for 2 min and resorption pits were observed under a bright-field microscope as clear zones in the matrix. Percentage resorption was calculated by considering the area of single well as 100% with six to eight wells per group.

RNA extraction and analysis by RT-PCR

RNA was isolated using TRIzol reagent (Invitrogen) and total RNA (2 μg) was used for synthesis of cDNA by reverse transcription (cDNA synthesis kit; Invitrogen). cDNA were used for real-time PCR using SYBR Green master mix (Applied Biosystems) for 40 cycles on a StepOnePlus system (Applied Biosystems). Each cycle consisted of 30 s denaturation at 94°C, 30 s annealing at 58–60°C, and 30 s extension at 72°C, followed by a melt curve at the end. GAPDH was used as endogenous control. The primer sequences used were: TRAP (forward, 5′-GGAACTTCCCCAGCCCTTAC-3′, reverse, 5′-AGGTCTCGAGGCATTTTGGG-3′), integrin β_3 (forward, 5′-AGAATGC CTGCTTGCCCATGT-3′, reverse, 5′-TACGGGACACGCTCTGTTTCT-3′),

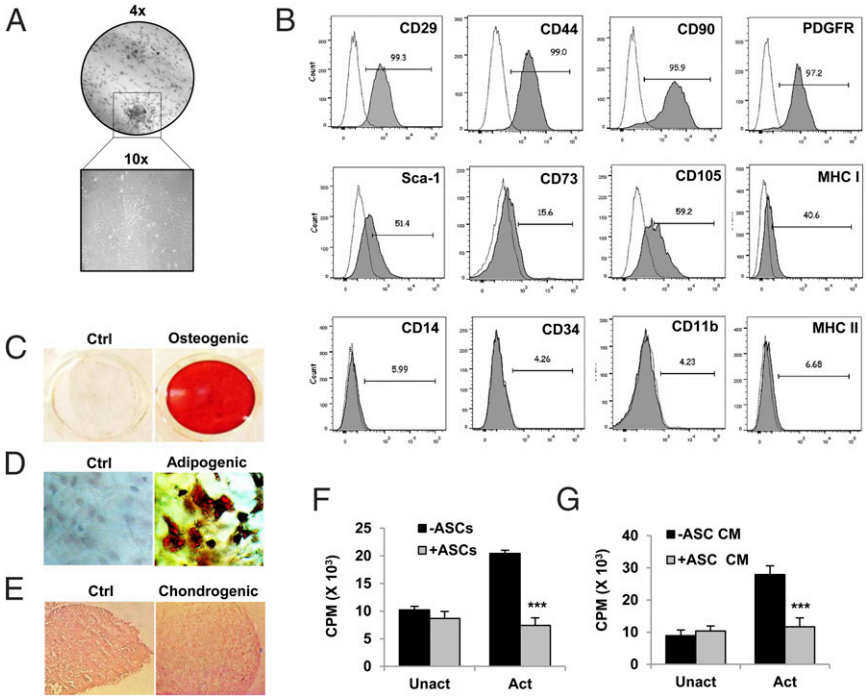

FIGURE 1. Culture-expanded murine ASCs exhibit multilineage differentiation and immunosuppressive potential. ASCs were isolated from s.c. adipose tissue of DBA/1J mice and culture expanded as described in *Materials and Methods*. (**A**) Cells of passage 2 were analyzed for their clonogenic potential by CFU-F assay. (**B**) Surface phenotyping for the expression of mesenchymal and hematopoietic markers by flow cytometry. Numbers indicate percentage expression of the marker with respect to their isotype controls. (**C**–**E**) Osteogenic, adipogenic, and chondrogenic differentiation of ASCs was induced in respective differentiation media. Matrix mineralization by differentiated osteoblasts was assessed by Alizarin red S staining. Adipocytes were characterized by Oil Red O staining. Chondrogenic differentiation shows cells in lacunae in H&E-stained sections of micromass pellet cultures (original magnification ×10). (**F**) Suppression of activated CD4$^+$ T cell proliferation by ASCs or (**G**) ASC-CM was assessed by coculturing splenic CD4$^+$ T cells (2.5×10^5 cells/ml) with ASCs (2.5×10^3 cells/ml) or ASC-CM (50% of culture volume) under activated or unactivated conditions for 72 h. T cell activation Dynabeads were used for activating T cells, and proliferation was measured by a [^{3}H]thymidine incorporation assay. Bar graphs are expressed as mean ± SEM of three to five replicates per group. ***$p \leq 0.001$. (A)–(E) are representative of more than five batches of ASCs. (F) and (G) are representative of two independent experiments.

calcitonin receptor (CTR; forward, 5′-TGCCAACCATTATCCACGCCA-3′, reverse, 5′-TCACAAGCACGCGGACAATGT-3′), dendritic cell–specific transmembrane protein (DC-STAMP; forward, 5′-AGAGCTGTTGACTTCC GGG-3′, reverse, 5′-ATACTTCCAGCCACAAGGGC-3′), cathepsin K (forward, 5′-TGCCTTCCAATACGTGCAGCA-3′, reverse, 5′-TGCATTTAGCT GCCTTTGCCG-3′), matrix metalloproteinase (MMP)9 (forward, 5′-CTGT CGGCTGTGGTTCA-3′, reverse, 5′-AGACGACATAGACGGCAT-3′), RANK (forward, 5′-TTCGACTGGTTCACTGCTCC-3′, reverse, 5′-CCTCA GAATCCACCGTGCTT-3′), c-fms (forward, 5′-ACAAGGCAGGCTGGAA TAAT-3′, reverse, 5′-TGGGCTTCATCACACCTATC-3′), and GAPDH (forward, 5′-GGTGCTGAGTATGTCGTG-3′, reverse, 5′-CCTTCCACATG CCAAAG-3′). Analysis was done by the comparative C_T method and fold change was calculated by the $2^{-\Delta\Delta CT}$ method.

Microcomputed tomography

Microcomputed tomography (μCT) of excised bones was carried out by a SkyScan 1076 CT scanner (SkyScan, Aartselaar, Belgium) as described previously for mice bone (23, 24) and following the general guidelines used for assessment of bone microarchitecture in rodents using μCT (25). Briefly, scanning was done at 50 kV, 200 μA using a 0.5-mm aluminum filter at a resolution of 9 μm/pixel. Reconstruction of sections was achieved using a modified Feldkamp cone-beam algorithm with beam hardening correction set to 50%. CT Analyzer software was employed for morphometric quantification of trabecular bone indices such as volumetric bone mineral density (BMD; g/cm^3), trabecular bone volume fraction (BV/TV %), trabecular number (Tb. N; 1/mm), trabecular thickness (Tb. Th; mm), trabecular separation (Tb. Sp; mm), and connectivity density (Conn. D; 1/mm^3). Cortical bone was also analyzed for BMD (cortical BMD [Ct. BMD]) and cross-sectional thickness (Cs. Th; mm).

Statistical analysis

Results are expressed as mean ± SEM or mean ± SD for various experimental groups. The statistical differences were analyzed using an unpaired Student *t* test for comparison between two groups or by a one- or two-way ANOVA followed by a Bonferroni correction for multiple comparisons. A p value <0.05 was considered statistically significant.

Results

Culture-expanded murine ASCs exhibit multilineage differentiation and immunosuppressive potential

We used ASCs from DBA/1J mice for the present study because of their high proliferation rate and attainment of homogeneity in cultures at early passages. ASCs from initial passages (P2 or P3) were characterized for their clonogenicity, expression of MSC markers, and multilineage differentiation. ASCs exhibited fibroblast-like morphology in culture, and their clonogenic potential was confirmed by classical CFU-F assay (Fig. 1A). These cells were strongly positive for surface expression of MSC markers CD90,

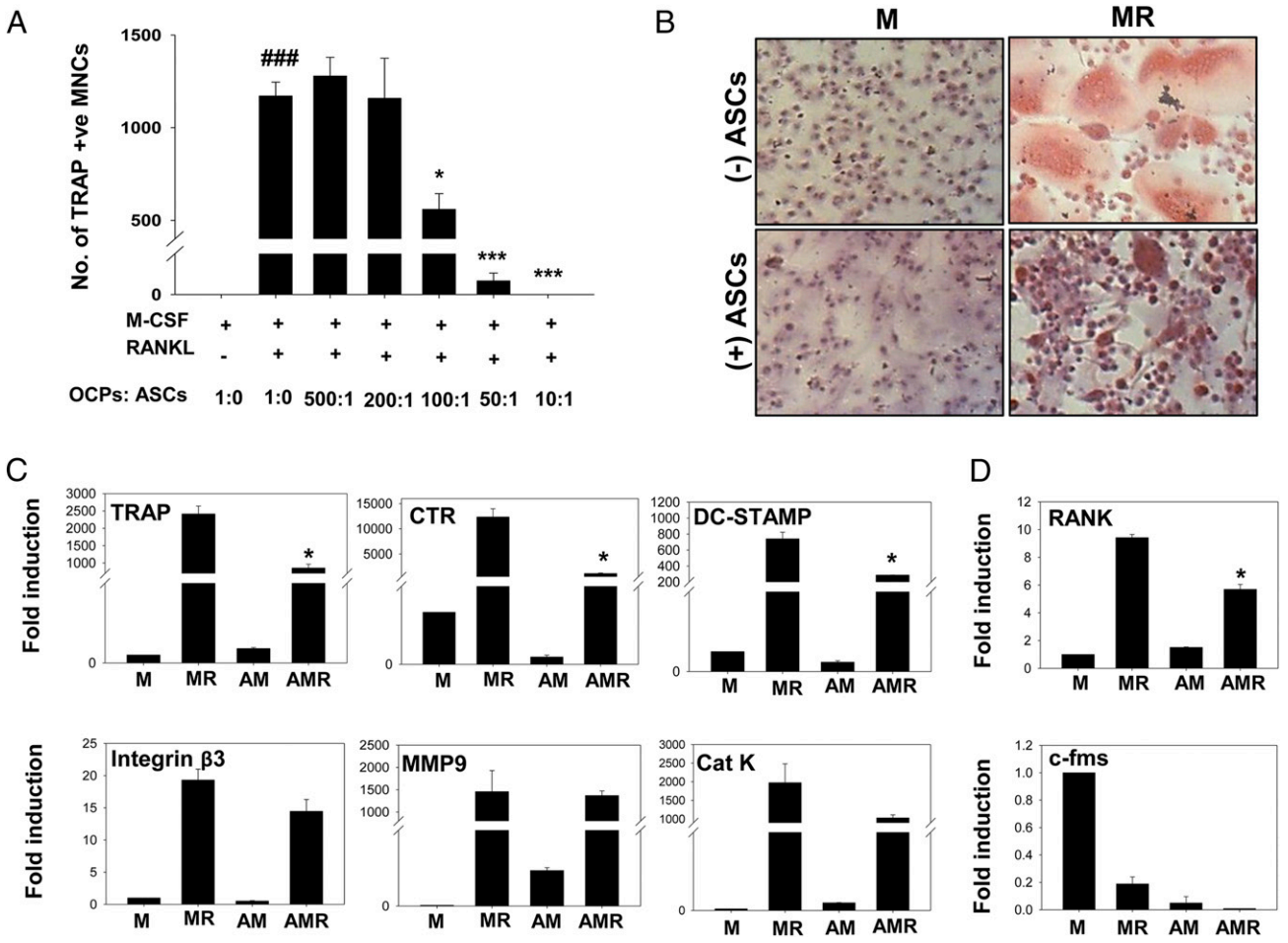

FIGURE 2. ASCs inhibit RANKL-induced osteoclast differentiation in vitro. M-CSF–dependent OCPs derived from bone marrow of DBA/1J mice were cultured in the presence of M-CSF (M, 30 ng/ml) and RANKL (R, 40 ng/ml) with or without ASCs. (**A**) OCPs (1×10^5 cells/well) were cultured in 48-well plates with graded ratios of ASCs, from 500:1 (OCP/ASC) to 10:1 and number of osteoclasts were counted as TRAP$^+$ MNCs (three or more nuclei). The p values are with respect to M-CSF and RANKL group without ASCs. (**B**) Representative images of coculture at an OCP/ASC ratio of 50:1, stained for TRAP and counterstained with hematoxylin (original magnification ×10). (**C**) Markers of osteoclast formation and function, namely TRAP, CTR, DC-STAMP, integrin β_3, MMP9, and cathepsin K (Cat K), were measured at the mRNA level by real-time PCR. (**D**) RANK and c-fms expression was also measured by quantitative PCR. Results are representative of two independent experiments. $^{###}p \leq 0.001$ compared with M-CSF group; $^{*}p \leq 0.05$, $^{***}p \leq 0.001$ compared with M-CSF and RANKL group. AM, M-CSF with ASCs; AMR, M-CSF and RANKL with ASCs; M, M-CSF; MR, M-CSF and RANKL.

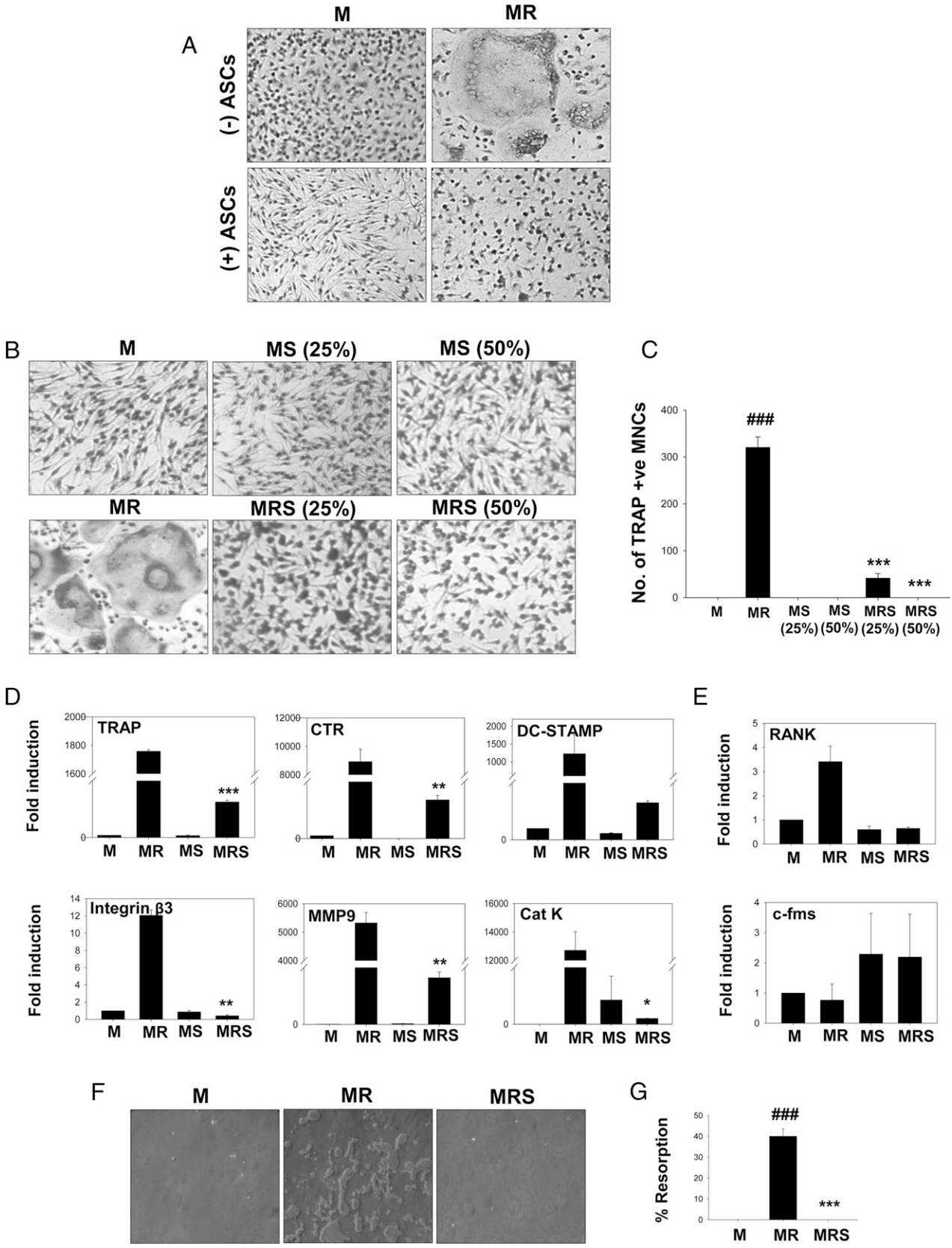

FIGURE 3. ASCs inhibit RANKL-induced osteoclast differentiation in a contact-independent manner. OCPs from mouse bone marrow were cultured in the presence of M-CSF and RANKL with or without ASCs in a contact-independent manner. (**A**) Representative photographs of TRAP$^+$ MNCs of Transwell cultures of osteoclast differentiation with OCPs in the lower chamber and ASCs in culture inserts. Original magnification ×10. Representative images (original magnification ×10) (**B**) and number of osteoclasts (**C**) in cultures where OCPs (5×10^4 cells/well) were differentiated into osteoclasts in 96-well plates in the presence or absence of ASC-CM (S) for 3–4 d are shown. ASC-CM was added at two different concentrations (25% and 50%). Gene expression analysis of markers of osteoclasts (**D**) and receptors of OCPs (**E**) is shown. Results are representative of three (A–C) and two (D and E) independent experiments. (**F** and **G**) OCPs were differentiated in 96-well plates coated with a calcium phosphate film, with or without 50% (*Figure legend continues*)

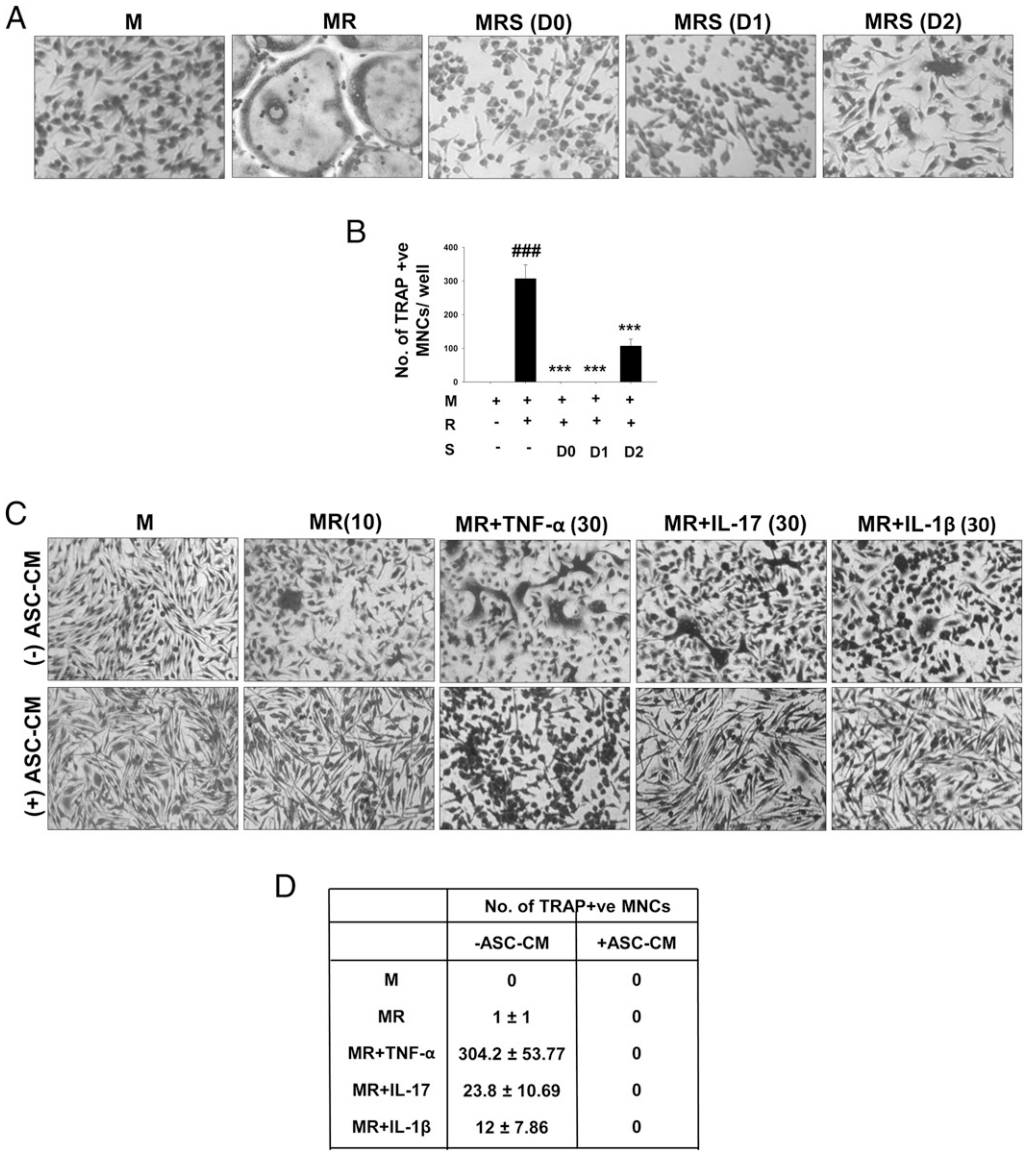

D

	No. of TRAP+ve MNCs	
	-ASC-CM	+ASC-CM
M	0	0
MR	1 ± 1	0
MR+TNF-α	304.2 ± 53.77	0
MR+IL-17	23.8 ± 10.69	0
MR+IL-1β	12 ± 7.86	0

FIGURE 4. ASC-CM potently inhibits osteoclastogenesis. M-CSF–dependent OCPs were differentiated into osteoclasts using M-CSF (30 ng/ml) and RANKL (40 ng/ml). ASC-CM was added at three different time points along the course of differentiation, that is, on days 0, 1, and 2. Cultures were fixed after 4 d and stained for TRAP. Representative images (**A**) and numbers (**B**) of osteoclasts in the cultures are shown (original magnification ×10). $^{###}p \leq 0.001$ compared with M-CSF group; $^{***}p \leq 0.001$ compared with M-CSF and RANKL group. (**C** and **D**) OCPs were cultured using M-CSF and RANKL (10 ng/ml) with or without proinflammatory cytokines TNF-α, IL-17, and IL-1β at a concentration of 30 ng/ml. ASC-CM was added to these cultures at 50% volume. Cultures were terminated after 3 d and stained for TRAP (original magnification ×10). Numbers are represented as mean ± SEM of five replicates in each group. Data are shown as representative images (C) and numbers of osteoclasts (D) of two independent experiments. M, M-CSF; MR, M-CSF and RANKL; MRS, M-CSF and RANKL with ASC-CM.

CD44, CD29, platelet-derived growth factor receptor, Sca-1, CD73, and CD105 and were negative for the hematopoietic marker CD34 and monocyte/macrophage markers CD14 and CD11b. These cells expressed MHC class I but not MHC class II, suggesting their compatibility for allogenic transplantation (Fig. 1B). The multilineage differentiation potential was determined by culturing ASCs in lineage-specific conditions. ASCs formed mineralized nodules in the presence of osteogenic factors, confirmed by Alizarin red S staining (Fig. 1C). Upon adipogenic induction for six or seven cycles of induction and maintenance, oil globules were formed within cells confirmed by Oil Red O staining (Fig. 1D). For chondrogenic differentiation, micromass pellets of ASCs were cultured in the presence of chondrogenic media for 21 d. Histological examination of H&E-stained sections of pellets showed differentiated chondrocytes present in the lacunae (Fig. 1E). To check the immunosuppressive potential of ASCs, we measured the proliferation of activated $CD4^+$ T cells in the presence or absence of ASCs or ASC-CM. For this, splenic $CD4^+$ T cells (2.5×10^5

ASC-CM (S) for 8 d. Cells were washed off and resorption of the calcium phosphate film by osteoclasts was assessed by bright-field microscopy. Original magnification ×10. Data are shown as representative images (F) and percentage resorption (G) of two independent experiments with eight replicates in each. $^{###}p \leq 0.001$ compared with M-CSF group; $^{*}p \leq 0.05$, $^{**}p \leq 0.01$, $^{***}p \leq 0.001$ compared with M-CSF and RANKL group. M, M-CSF; MR, M-CSF and RANKL; MRS, M-CSF and RANKL with ASC-CM; MS, M-CSF with ASC-CM.

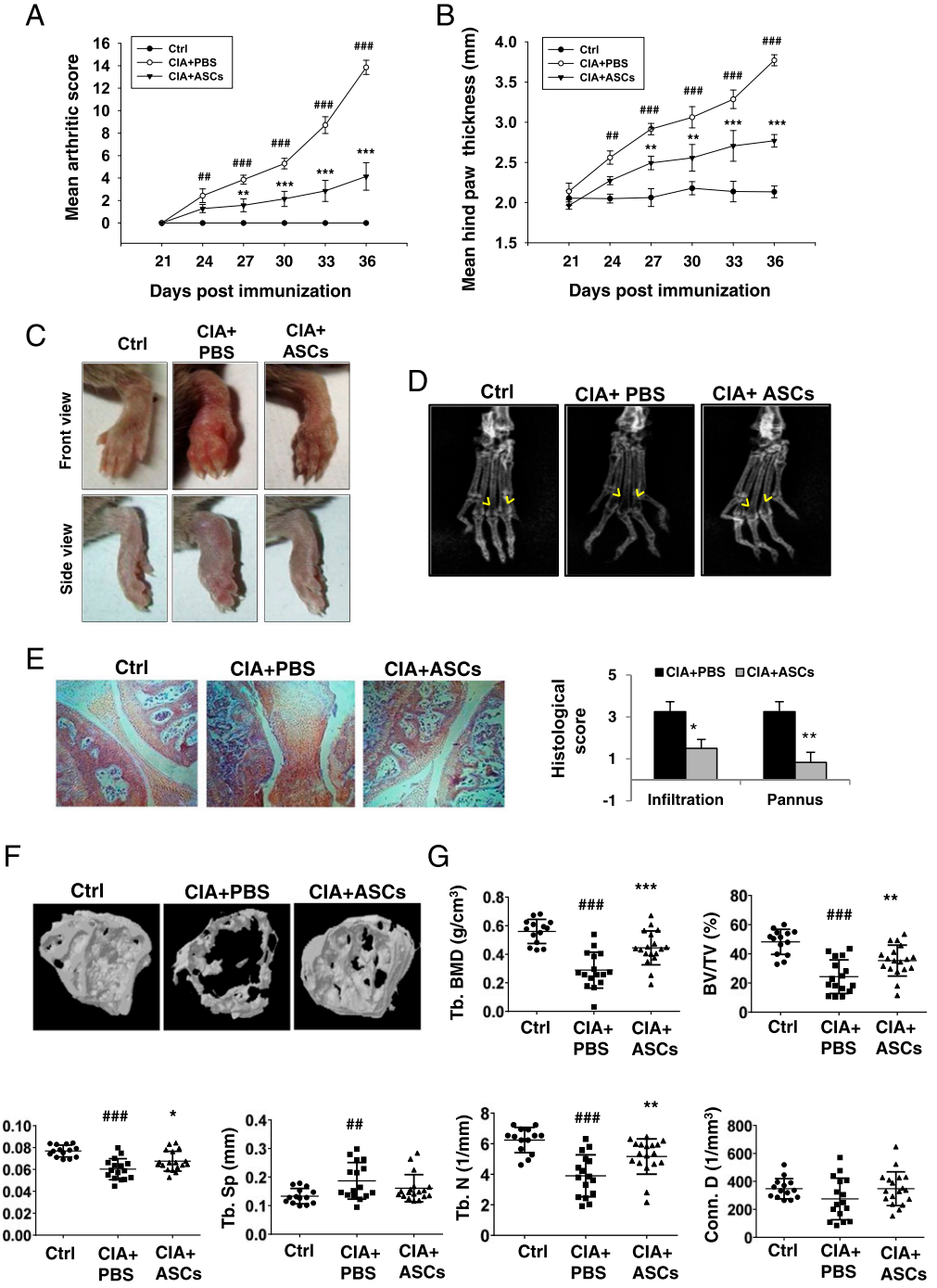

FIGURE 5. ASCs decrease the disease severity and bone destruction in CIA. CIA was induced in 8- to 10-wk-old DBA/1J mice as described in *Materials and Methods*. On day 22, 2×10^6 ASCs in 100 μl PBS were injected i.p. to one group and an equal volume of PBS to the other group of CIA mice. Severity of arthritis was evaluated by measuring mean arthritic score of four limbs per animal (**A**) and hindpaw thickness (**B**) until day 36. Data are presented as mean ± SEM (n = 6–7/group). Significance was calculated by two-way ANOVA followed by a Bonferroni multiple comparisions test between 1) control versus CIA plus PBS groups and 2) CIA plus PBS versus CIA plus ASC groups. Similar results were obtained in four independent experiments. Representative images (**C**) and radiographs (**D**) of hindpaws of mice on day 36 are shown. Yellow arrows in (D) show bone density at the metatarsophalangeal joints. (**E**) Sections of knee joints were stained with H&E and histologically evaluated for cellular infiltration and pannus formation (n = 4–6 mice/group). Original magnification ×10. Significance was calculated by a Student t test between CIA plus PBS and CIA plus ASC groups. Similar results were obtained in three independent experiments. Hindlimbs along with ankle joints were dissected out and analyzed for histomorphometric measurements using μCT. (**F**) Representative three-dimensional images of distal tibiae from control (nonarthritic), PBS-treated, and ASC-treated CIA mice. (**G**) Trabecular bone indices, including volumetric bone mineral density (trabecular BMD [Tb. BMD]), BV/TV, Tb. Th, Tb. Sp, Tb. N, and Conn. D, were quantified from μCT reconstructions. Data are pooled from three independent experiments and are presented as mean ± SD of 14–18 mice per group. Significance was calculated by a one-way ANOVA with a Bonferroni multiple comparisons test between 1) control versus CIA plus PBS groups and 2) CIA plus PBS versus CIA plus ASC groups. $^{\#\#}p \leq 0.01$, $^{\#\#\#}p \leq 0.001$ with respect to control group; $^{*}p \leq 0.05$, $^{**}p \leq 0.01$, $^{***}p \leq 0.001$ with respect to CIA plus PBS group.

cells/ml) were cultured with either ASCs (2.5×10^3 cells/ml) or ASC-CM (50% of culture volume) for 72 h along with T cell activation Dynabeads. T cell proliferation was measured by a [^{3}H]thymidine incorporation assay. ASCs (Fig. 1F) as well as ASC-CM (Fig. 1G) inhibited proliferation of activated CD4$^+$ T cells under in vitro conditions. These results indicate the clonogenic,

multilineage differentiation and immunosuppressive properties of isolated ASCs. ASCs of passages two or three were used in all further experiments.

ASCs inhibit RANKL-induced osteoclastogenesis in vitro in both a contact-dependent and -independent manner

The effect of MSCs on osteoclast differentiation has not been well studied in either mice or humans. To investigate the role of ASCs on in vitro osteoclastogenesis, we differentiated mouse bone marrow–derived M-CSF–dependent OCPs into multinuclear osteoclasts, using M-CSF (30 ng/ml) and RANKL (40 ng/ml). ASCs were added to cultures in increasing ratios ranging from 200 to 10,000 cells per well, keeping numbers of OCPs (1×10^5 cells/well) constant. After 3 d, cells were stained for TRAP, and $TRAP^+$ multinuclear cells (MNCs) with three or more nuclei were counted as osteoclasts. We observed that ASCs significantly decreased the number of osteoclasts at a minimal OCP/ASC ratio of 100:1, with complete absence of osteoclasts at an OCP/ASC ratio of 10:1 (Fig. 2A). M-CSF–treated OCPs without RANKL served as control with no osteoclasts, and no deleterious effect on mononuclear cells was seen in the presence of ASCs (Fig. 2B). The inhibition of osteoclast differentiation was further assessed by analyzing markers associated with osteoclast differentiation and activation at the transcript level. Osteoclast markers such as TRAP, CTR, and DC-STAMP were significantly downregulated in cocultures with ASCs (Fig. 2C). Expression of integrin β_3, MMP9, and cathepsin K was also decreased to some extent by ASCs. Notably, ASCs alone did not induce osteoclast differentiation, as indicated by the absence of $TRAP^+$ MNCs (Fig. 2B) and osteoclast markers (Fig. 2C) in cultures without RANKL. The receptor for RANKL, RANK, was also downregulated by ASCs, and c-fms, the receptor for M-CSF, did not show any significant change in its expression in the presence of ASCs (Fig. 2D).

To check whether the observed inhibitory effect of ASCs on osteoclastogenesis was cell–cell contact-dependent or -independent, we set up Transwell assays, where ASCs were separated from OCPs using 0.8-μm culture inserts. ASCs were added in the upper chamber and OCPs in the lower chamber along with M-CSF and RANKL for 3 d. ASCs retained the inhibitory effect on osteoclast differentiation, indicating the involvement of soluble mediators in the inhibition of osteoclastogenesis (Fig. 3A). In support of this, ASC-CM also inhibited the formation of $TRAP^+$ MNCs. ASC-CM at 25% volume partially inhibited osteoclast differentiation whereas complete inhibition was seen at 50% volume (Fig. 3B, 3C). The inhibition was further confirmed by downregulation of osteoclast markers at the mRNA level (Fig. 3D). ASC-CM did not affect the expression of RANK and c-fms on OCPs as analyzed by real-time PCR (Fig. 3E). We also differentiated OCPs in the presence or absence of ASC-CM in 96-well plates coated with a thin film of calcium phosphate for 8 d. No clear zones of resorption were formed in the presence of ASC-CM, further confirming inhibition of osteoclast formation (Fig. 3F, 3G).

To determine the stage at which osteoclast differentiation was affected by ASC-CM, we cultured OCPs with M-CSF and RANKL, and ASC-CM (50%) was added on days 0, 1, and 2. Cultures were fixed and stained for TRAP on day 4. We observed complete inhibition of osteoclast formation when ASC-CM was added on days 0 and 1, and significant inhibition was also seen when ASC-CM was added on day 2 (Fig. 4A, 4B). All these in vitro data clearly indicate a strong anti-osteoclastogenic potential of ASCs in vitro.

Proinflammatory cytokines, such as TNF-α, IL-17, and IL-1, are present at the sites of inflammatory bone erosions, and they act synergistically with RANKL in enhancing osteoclastogenesis (3, 26, 27). We further evaluated whether ASCs can inhibit osteoclastogeneis in the presence of these proinflammatory cytokines. OCPs were differentiated with M-CSF (30 ng/ml) and low concentration of RANKL (10 ng/ml) along with 30 ng/ml TNF-α, IL-17, or IL-1β. ASC-CM was added at 50% volume to these cultures. We observed that TNF-α strongly synergized with RANKL and induced the formation of many giant osteoclasts. IL-17 and IL-1β also enhanced formation of multinuclear osteoclasts. Interestingly, ASC-CM inhibited osteoclastogenesis in the presence of all the proinflammatory cytokines (Fig. 4C, 4D). These results indicate a potent inhibitory effect of ASCs on osteoclastogenesis.

ASCs reduce disease severity and bone destruction in CIA mice

Having demonstrated the potential of ASCs in inhibiting osteoclastogenesis in the presence of proinflammatory cytokines, we wanted to validate this in an in vivo model of inflammation-induced bone loss. The CIA model shares many pathological features with human RA, including synovial hyperplasia, joint swelling, bone and cartilage destruction, and autoimmune T cell responses. CII, the main component of articular cartilage, is given as the autoantigen in this model (28). Genetically susceptible DBA/1J mice were immunized with CII emulsified in CFA on day 0, and an equal amount of CII emulsified in IFA was given as a booster dose on day 21. One day after the booster dose, mice received i.p. injections of 2 million murine syngeneic ASCs in 100 μl PBS or PBS alone. Mice of similar age group and gender were taken as normal controls. Mice were assessed for clinical symptoms every third day from day 21 until day 36 of the initial immunization. In control CIA mice, symptoms started to appear from day 24 and reached a score of >10 per animal by day 36. However, mice treated with ASCs developed a less severe form of arthritis as seen by decreased mean arthritic score (Fig. 5A) and hindpaw thickness (Fig. 5B). Images (Fig. 5C) of hindpaws of mice showed significant reduction in inflammation and soft tissue swelling, and radiographs (Fig. 5D) showed reduced bone erosions in the metatarsophalangeal joints upon treatment with ASCs. Mice were sacrificed on day 36 for histopathological examination of joints. Reduced severity of arthritis in ASC-treated mice was associated with decreased infiltration of immune cells and pannus formation in affected joints (Fig. 5E). Histological analysis also revealed reduced subchondral bone erosions in ASC-treated mice. To further evaluate the effect on local bone destruction, epiphyseal trabecular bone of distal tibia was subjected to μCT analysis. ASCs protected the collagen-immunized animals from severe bone destruction as seen in representative μCT images (Fig. 5F) and histomorphometric measurements (Fig. 5G). Loss of volumetric BMD, BV/TV, Tb. Th, and Tb. N in CIA mice was significantly prevented in mice treated with ASCs (Fig. 5G). Increased Tb. Sp in CIA mice was also slightly decreased upon treatment with ASCs (Fig. 5F). These data indicate that ASCs reduce clinical symptoms, joint pathology, and local bone destruction in CIA mice.

ASCs decrease periarticular and systemic osteopenia in CIA mice

Inflammatory processes in RA result in adverse effects on bone remodeling, skewing the balance toward resorption. The effect of ASCs on inflammation-induced periarticular and systemic bone loss was assessed by μCT of trabecular and cortical bone structures. The distal femur and fifth lumbar vertebra (L5) were analyzed for BMD and trabecular bone parameters. Additionally, cortical bone at femur mid-diaphysis was analyzed. Arthritis was associated with an increase in trabecular bone loss in the metaphyseal region of both distal femur (Fig. 6A, 6B) and proximal tibia (data not shown). Representative images (Fig. 6A) and histomorphometric measurements (Fig. 6B) of cancellous bone of distal femora of control nonarthritic, PBS-treated, and ASC-treated CIA

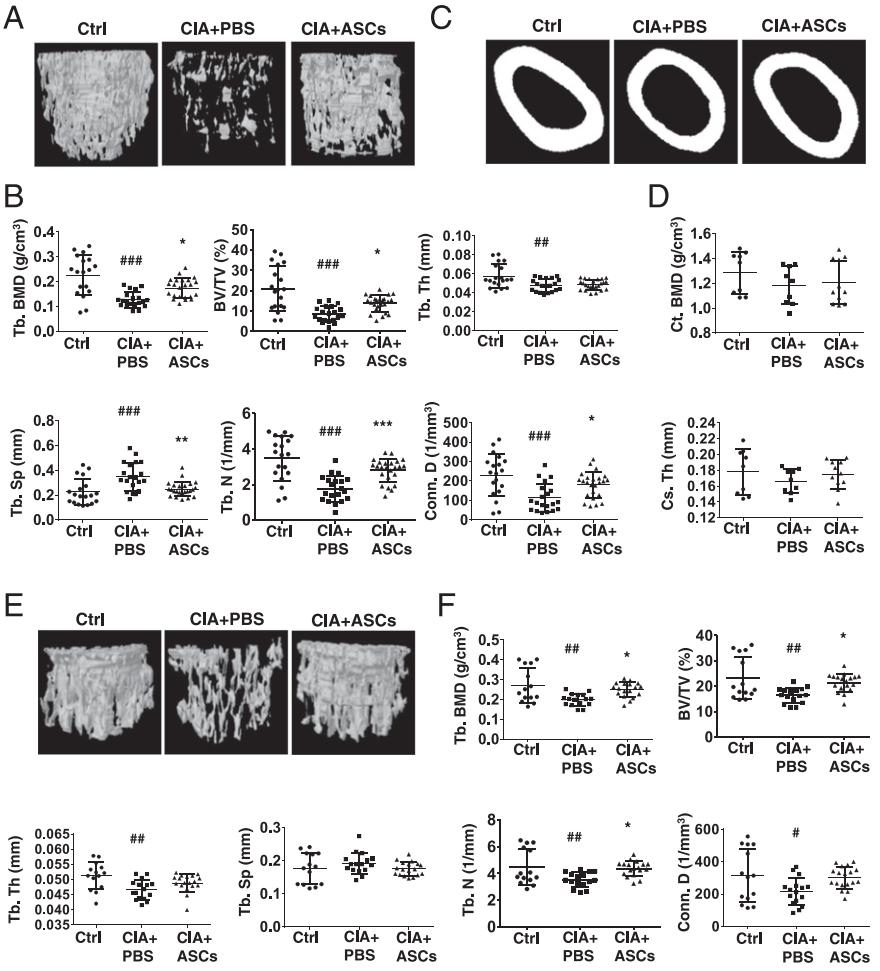

FIGURE 6. ASCs protect from periarticular and systemic bone loss in CIA mice. CIA mice were injected i.p. with PBS or 2×10^6 ASCs on day 22 of primary immunization and sacrificed on day 36. (**A**) Representative three-dimensional images of distal femur from control nonarthritic, PBS-treated, and ASC-treated CIA mice. (**B**) Trabecular bone indices, including Tb. BMD, BV/TV, Tb. Th, Tb. Sp, Tb. N, and Conn. D, were quantitated from μCT reconstructions. Data are pooled from three independent experiments and are presented as mean ± SD of 14–18 mice per group. Representative two-dimensional images (**C**) and quantitative measurements (**D**) of femur middiaphysis Ct. BMD and Cs. Th are shown. Data are pooled from two independent experiments and are presented as mean ± SD of 9–11 mice per group. Representative three-dimensional images (**E**) and trabecular parameters (**F**) of the fifth lumbar vertebra (L5) are shown. Data are pooled from three independent experiments and are presented as mean ± SD of 14–18 mice per group. Significance was calculated by a one-way ANOVA with a Bonferroni multiple comparisons test between 1) control versus CIA plus PBS groups and 2) CIA plus PBS versus CIA plus ASC groups. $^{\#}p \leq 0.05$, $^{\#\#}p \leq 0.01$, $^{\#\#\#}p \leq 0.001$ with respect to control group; $^{*}p \leq 0.05$, $^{**}p \leq 0.01$, $^{***}p \leq 0.001$ with respect to CIA plus PBS group.

mice showed protection of trabecular structure in ASC-treated mice compared with PBS-treated arthritic controls. A significant increase in trabecular bone indices, including trabecular BMD (Tb. BMD), BV/TV, Tb. N, and Conn. D, was observed in ASC-treated mice with respect to PBS-injected CIA mice. Increased Tb. Sp in CIA mice was significantly decreased by ASC treatment (Fig. 6B). A similar pattern was observed in BV/TV, Tb. Sp, and parameters of trabecular microstructure of tibiae (data not shown). Femoral middiaphyseal scanning showed no significant difference in Ct. BMD and Cs. Th between the groups (Fig. 6C, 6D). We also performed μCT of L5 (mostly consisting of trabecular bone) to evaluate the effect of ASC treatment on axial skeleton. Significant bone loss was seen in CIA mice compared with normal controls, and treatment with ASCs significantly prevented this loss, indicated by increased BMD and improved trabecular parameters (Fig. 6E, 6F). All of these data confirm a strong protective effect of ASCs on inflammation-induced bone loss in CIA mice.

ASCs decrease osteoclastogenesis in arthritic mice by reducing osteoclast precursors

We next investigated the mechanisms underlying decreased severity of arthritis and bone loss upon treatment with ASCs. To study the levels of osteoclastogenesis in ASC-treated mice, bone marrow–derived stromal cell-free OCPs from all three groups of mice were differentiated into osteoclasts using M-CSF and two different concentrations of RANKL (25 and 50 ng/ml) ex vivo. CIA mice showed increased osteoclast numbers compared with control mice at a higher concentration of RANKL (50 ng/ml). Although there was no significant difference in the number of osteoclasts at a lower concentration of RANKL (25 ng/ml), the size of osteoclasts of CIA mice was bigger compared with normal mice. Similarly, the increased size of osteoclasts explains the decrease in their numbers at a concentration of 50 ng/ml RANKL. Osteoclast numbers were decreased in ASC-treated CIA mice compared with PBS-treated ones at both concentrations of RANKL (Fig. 7A, 7B). The decreased osteoclastogenesis in ASC-injected mice could be a result of either decreased numbers of osteoclast precursors or RANK expression on precursors, leading to a decreased sensitivity toward RANKL. The percentage of OCPs, indicated by the $CD11b^{+}$c-fms^{+} population, was higher in PBS-treated CIA mice compared with normal controls, which was significantly decreased in CIA mice treated with ASCs (Fig. 7C). However, no significant change was observed in their RANK expression (Fig. 7D). Absence of significant changes in the percentages of $F4/80^{+}$ macrophages (Supplemental Fig. 1A), $CD11c^{+}$ dendritic cells (Supplemental Fig. 1B), and c-Kit^{+} myeloid progenitors (Supplemental Fig. 1C) in all three groups of mice implies lack of deleterious effect of ASCs on other myeloid populations of bone marrow. These results indicate that enhanced osteoclastogenesis in CIA mice was reduced upon treatment with ASCs as a result of decreased osteoclast precursor pool.

ASCs promote immune tolerance in CIA mice by reducing autoimmune T cell proliferation and enhancing regulatory lymphocyte population

Autoimmune T and B cell responses against CII lead to systemic inflammation, which subsequently drives bone destruction in CIA (28). However, a regulatory subset of T cells (Tregs) is involved in inducing tolerance and confers protection against CIA by preventing autoimmune responses (29) and bone loss (30). We observed that treatment of CIA mice with ASCs inhibited proliferation of dLN

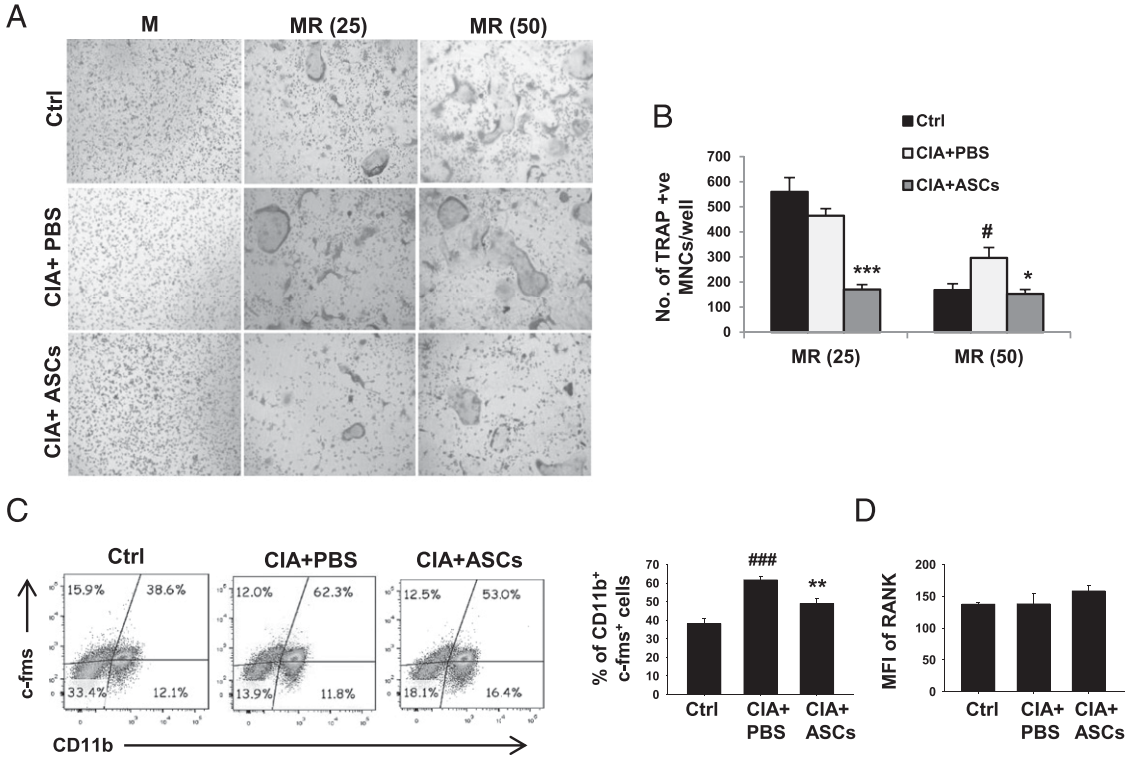

FIGURE 7. ASCs decrease RANKL-induced osteoclastogenesis in CIA mice by reducing osteoclast precursors. CIA mice were injected i.p. with PBS or 2×10^6 ASCs on day 22 of the first immunization and sacrificed on day 36. Bone marrow was harvested and M-CSF–dependent OCPs were differentiated into osteoclasts in the presence of M-CSF with or without two different concentrations of RANKL (25 or 50 ng/ml). Representative images (**A**) and numbers of osteoclasts (**B**) in cultures are shown as a measure of osteoclastogenesis (original magnification ×10). (**C**) Percentage of osteoclast precursors ($CD11b^+c\text{-}fms^+$) in bone marrow. (**D**) The amount of RANK expressed on $CD11b^+$ cells of bone marrow. Data are presented as mean ± SEM of seven mice per group in (B), four to five mice per group in (C), and five mice per group in (D). Significance was calculated by a one-way ANOVA with a Bonferroni multiple comparisons test between 1) control versus CIA plus PBS groups and 2) CIA plus PBS versus CIA plus ASC groups. Similar results were obtained in three independent experiments. $^{\#}p \leq 0.05$, $^{\#\#\#}p \leq 0.001$ with respect to control group; $^{*}p \leq 0.05$, $^{**}p \leq 0.01$, $^{***}p \leq 0.001$ with respect to CIA plus PBS group. M, M-CSF; MR, M-CSF and RANKL.

cells in response to CII (40 ng/ml), compared with PBS treatment, as indicated by stimulation indices (Fig. 8A). Non–Ag-specific T cell proliferation measured in response to anti-CD3ε was also significantly reduced upon treatment with ASCs compared with PBS controls (Fig. 8A). This confirmed that ASCs markedly suppressed autoimmune T cell responses in CIA mice. ASCs, when cocultured with $CD4^+$ T cells for 5 d under activation conditions, induced regulatory phenotype in T cells (Fig. 8B). Percentages of Tregs indicated by $CD4^+Foxp3^+$ dual-positive population in peritoneum, synovium, peripheral blood, and dLNs were significantly increased upon ASC treatment, compared with PBS-treated arthritic mice. However, the percentage of splenic Tregs was unaffected (Fig. 8C). These results indicate immunosuppressive and tolerogenic potential of ASCs in CIA mice. B cell depletion inhibits CIA, suggesting the involvement of B cells and autoantibodies in the pathogenesis of CIA (31). However, Bregs with the $CD19^+CD1d^{hi}CD5^+$ phenotype were shown to possess protective effect in autoimmune disease models (32). We found an increase in the percentage of the splenic Breg subset in CIA mice upon treatment with ASCs (Fig. 8D). The serum levels of total anti-CII IgG Ab were unaffected in ASC-treated mice compared with PBS-treated animals (Fig. 8E). These results suggest that ASCs promote immune tolerance by increasing the number of regulatory lymphocytes in CIA mice.

Discussion

Human RA is a complex disease affecting multiple systems in the body, predominantly inflammatory synovitis and structural damage to bone. Also, RA is an independent risk factor for generalized osteopenia and osteoporosis leading to systemic bone loss. Although reduction in inflammatory synovitis can be achieved by conventional antirheumatics, protection against structural damage requires complete abrogation of inflammation. This may lead to severe immune suppression posing a threat of infections to the treated individuals. The uncoupling of inflammation and bone erosion processes in few individuals (33) further complicates the treatment strategy, rendering anti-inflammatory agents ineffective in preventing the structural damage to bone. Therefore, the agents affecting both inflammatory and skeletal components of the disease can be effective treatment strategies in such conditions. MSCs have emerged as a promising therapeutic candidate in various autoimmune and degenerative diseases, with significant improvement in pilot scale clinical trials. Although the immunomodulation by MSCs in RA is well studied, the effect on bone destruction associated with disease has not been understood. In this study, we used a homogeneous population of ASCs having both differentiation and immunosuppressive properties, and we investigated their effect on bone loss along with autoimmune responses in CIA mice.

The role of osteoclast activation in systemic osteoporosis associated with inflammatory arthritis has been verified in various animal models. Inhibiting osteoclast differentiation and function becomes an important part of the treatment regimen when bone destruction is the therapeutic target. We observed a strong inhibitory potential of ASCs on RANKL-induced osteoclast differentiation in both a contact-dependent and -independent manner. Previously, murine MSCs derived from compact bone have been shown to promote osteoclastogenesis in vitro through expression

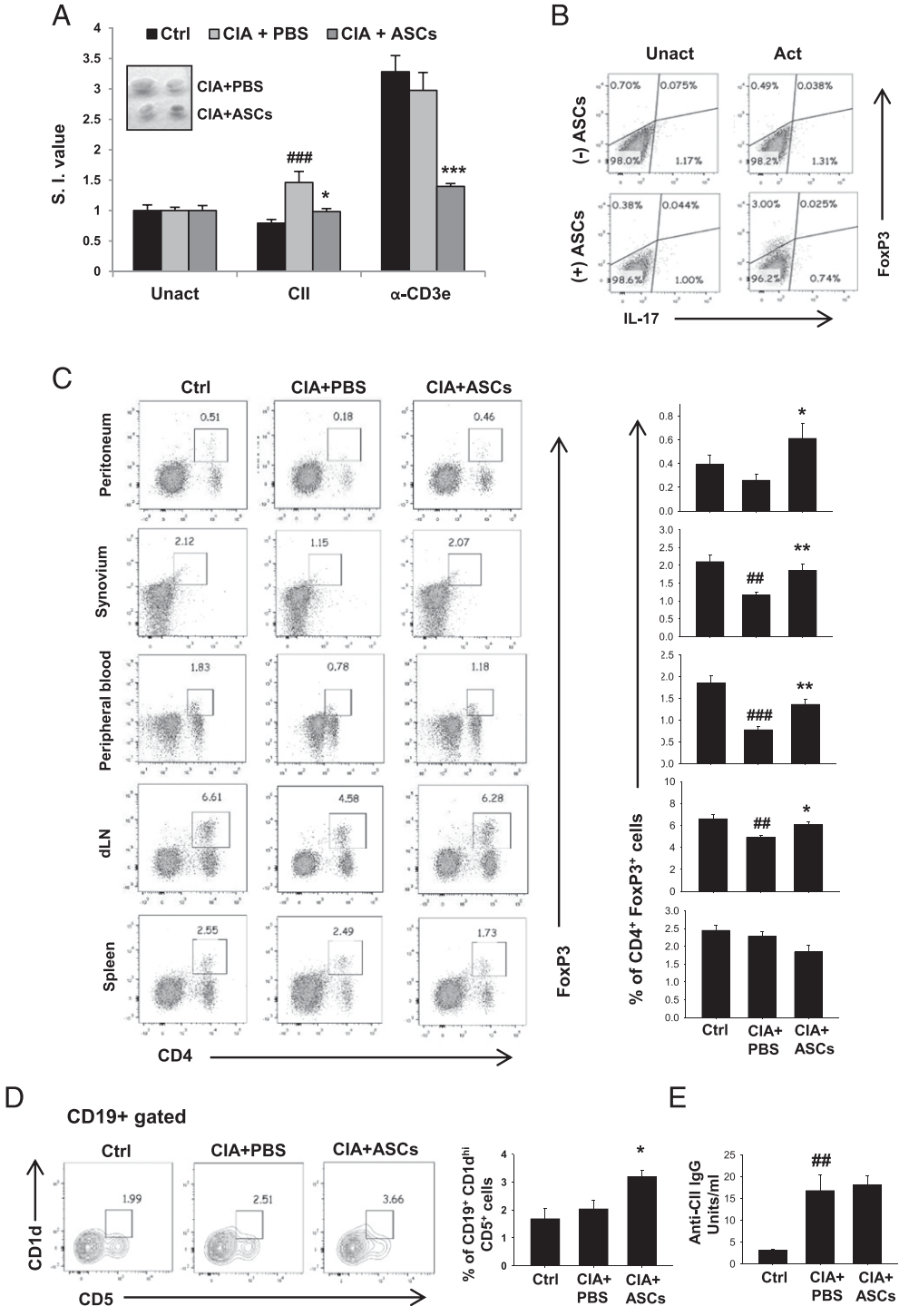

FIGURE 8. ASCs reduce CII-specific T cell proliferation and induce regulatory lymphocytes in arthritic mice. CIA mice were injected with PBS or 2×10^6 ASCs on day 22 of initial immunization. On day 36, mice were sacrificed and analyzed for immune parameters. (**A**) dLN cells were cultured in the presence of CII (40 μg/ml) or plate-bound anti-CD3ε (2 μg/ml) for 72 h and proliferation was measured by [^{3}H]thymidine incorporation assay. Stimulation indices (S.I.) values are calculated using the formula: cpm in response to Ag/cpm in absence of Ag. The *inset* in (A) shows the representation of decreased size of dLNs in ASC-treated CIA mice compared with PBS-treated controls. (**B**) Magnetically sorted splenic CD4$^+$ T cells (5×10^5 cells/well) from DBA/1J mice were cultured with or without ASCs (5×10^3 cells/well) in 48-well plates for 72 h. Cells were stained for Foxp3 and IL-17A and analyzed by flow cytometry. Plots are representative of two independent experiments. (**C**) Representative plots and average percentages of CD4$^+$Foxp3$^+$ Tregs in the peritoneal cavity, synovium, peripheral blood, dLNs, and spleens of control, arthritic, and ASC-treated arthritic mice. (**D**) Percentages of CD1d^{hi}CD5$^+$ Bregs from CD19-gated population of splenocytes. (**E**) Anti-CII IgG titers were measured in serum by ELISA. Data are presented as mean ± SEM of six to seven mice per group in (A), five to seven mice per group in (C), three to six mice per group in (D), and four mice per group in (E). Significance was calculated by a one-way ANOVA with a Bonferroni multiple comparisons test between 1) control versus CIA plus PBS groups and 2) CIA plus PBS versus CIA plus ASC groups. Similar results were observed in two independent experiments. $^{\#\#}p \leq 0.01$, $^{\#\#\#}p \leq 0.001$ with respect to control group; $^*p \leq 0.05$, $^{**}p \leq 0.01$, $^{***}p \leq 0.001$ with respect to CIA plus PBS group.

of RANKL (17). In our study, murine ASCs alone could not induce osteoclast differentiation despite their expression of RANKL (data not shown). Based on our results and existing literature, the multilineage and T cell suppressive properties seem to be common among MSCs derived from all sources; however, there might be few tissue-specific functions that can be attributed to the variations in their anti-osteoclastogenic effect. Our results are in agreement with two other reports demonstrating the inhibitory effect of human bone marrow MSCs on in vitro osteoclastogenesis mediated through osteoprotegerin, a decoy receptor for RANKL, or through surface expression of CD200 (18, 19). Although our ASCs constitutively expressed osteoprotegerin (data not shown), the inhibitory effect of ASC-CM on osteoclast differentiation in the presence of high concentrations of RANKL (200 ng/ml) (data not shown) rules out its complete involvement in the inhibition of osteoclastogenesis. The complete mechanisms of inhibitory action of ASCs on osteoclast formation is not yet understood, but we speculate that it could be the concerted effect of all pro- and anti-osteoclastogenic molecules secreted by ASCs. Proinflammatory cytokines, such as TNF-α, IL-17, and IL-1, are present at the sites of inflammatory bone erosions and act synergistically with RANKL in enhancing osteoclastogenesis and bone loss (3, 26). The inhibitory effect of ASC-CM on the RANKL-induced osteoclast formation in the presence of these proinflammatory cytokines suggests a strong protective effect against inflammation-mediated bone destruction.

In our study, a single injection of murine ASCs at the onset of disease significantly reduced the severity of disease in CIA mice. Murine bone marrow MSCs have shown contradictory results in reducing the disease severity in CIA model, despite inhibiting T cell proliferation in response to CII (34–37). However, mouse and human ASCs have been reported to ameliorate CIA by modulating T cell responses (15, 38). It appears that MSCs from adipose tissue could be advantageous over those from bone marrow for the treatment of arthritis, although it needs to be supported by more experimental evidences.

CIA induced loss of trabecular bones at appendicular and axial sites as assessed by μCT, and treatment with ASCs protected arthritic bone loss. Trabecular parameters of L5 vertebrae were also significantly improved in ASC-treated mice compared with arthritic mice. These results suggested that ASC treatment protected not only periarticular but also systemic bone loss. Trabecular bone remodeling (turnover) units occur in much greater numbers due to high surface area/bone matrix volume configuration than the cortical bone, resulting in bone turnover rate at the trabecular sites being much higher than at the cortical sites (39). Therefore, increased osteoclastogenesis under any pathological condition such as the one we observed with CIA is more likely to result in the loss of trabecular bones over cortical bones as the remodeling event is triggered by osteoclasts. In the present study, cortical bone in the CIA group was maintained at the level of control whereas the trabecular bones suffered significant loss during the duration of this study. It is possible that a longer duration of CIA than the present 36 d could have induced cortical bone loss. In our study, treatment of arthritic mice with one dose of ASCs improved the trabecular bone parameters and mitigated bone loss. Based on the present data, it is reasonable to speculate that the extent of protection conferred against trabecular bone loss in CIA could be further improved by increased dosage or frequency of administration of ASCs.

In agreement with another study (40), there was an increase in the number of osteoclast precursors and osteoclastogenesis in CIA mice compared with normal controls. In the present study, the number of OCPs and the osteoclastogenic potential of bone marrow cells were decreased in CIA mice upon treatment with ASCs. ASCs decreased OCPs in bone marrow without affecting the percentage of other myeloid lineage cells, including $F4/80^+$ mature macrophages, $CD11c^+$ dendritic cells, and $CD11b^-$c-Kit^+ myeloid precursors.

In addition to increased osteoclastogenesis, bone formation is also compromised in arthritis at sites of focal bone erosion (4, 41). MSCs derived from mouse bone tend to lose their differentiation potential in the presence of proinflammatory cytokines (42). Also, lack of repair of bone erosion by antirheumatic drugs is due to active suppression of bone formation by proinflammatory cytokines (5). However, we observed an increased mineralization of ASCs in the presence of two major proinflammatory cytokines of arthritic synovium, TNF-α and IL-17 (Supplemental Fig. 2). These results suggest that ASCs are resistant to inhibitory action of these cytokines on osteoblast differentiation and bone formation.

Tregs play a crucial role in controlling autoimmunity by inducing tolerance, and they prevent the development of chronic inflammatory and autoimmune diseases (43). ASCs decreased T cell proliferation in CIA mice, measured in response to anti-CD3ε and CII, the main autoantigen in the model. ASCs also promoted Treg generation in peripheral tissues, including dLNs, peritoneum, synovium, and peripheral blood. The decreased autoimmune responses could be due to the direct effect of ASCs on T cell suppression or indirectly through increased Treg population. Tregs are also shown to inhibit osteoclastogenesis and protect bone destruction in arthritis (30, 44). The increased percentage of Tregs in ASC-treated mice could also have contributed to decreased osteoclastogenesis and bone loss in ASC-treated CIA mice. Thus, ASCs affected osteoclastogenesis and bone loss in CIA mice both directly and indirectly.

In addition to Tregs, we also observed an increase in the percentage of $CD19^+CD1d^{hi}CD5^+$ Bregs in the spleens of ASC-treated CIA mice compared with PBS-treated controls. Bregs were shown to have a protective effect in autoimmune disease models of experimental autoimmune encephalomyelitis and CIA (45, 46). Also, human bone marrow MSCs were shown to upregulate Bregs in an experimental autoimmune encephalomyelitis model (47). This suggests that Bregs also contribute to the protective effect of ASCs in RA. Thus, we demonstrate that ASCs inhibit pathological bone loss by suppressing osteoclastogenesis and improving immune tolerance in CIA mice. Our results suggest that ASCs have the potential to serve as better therapeutic agents for RA.

Acknowledgments

We thank Snehal R. Joshi for critically reading the manuscript.

Disclosures

The authors have no financial conflicts of interest.

References

1. Firestein, G. S. 2003. Evolving concepts of rheumatoid arthritis. *Nature* 423: 356–361.
2. Teitelbaum, S. L. 2000. Bone resorption by osteoclasts. *Science* 289: 1504–1508.
3. McInnes, I. B., and G. Schett. 2007. Cytokines in the pathogenesis of rheumatoid arthritis. *Nat. Rev. Immunol.* 7: 429–442.
4. Schett, G., and E. Gravallese. 2012. Bone erosion in rheumatoid arthritis: mechanisms, diagnosis and treatment. *Nat. Rev. Rheumatol.* 8: 656–664.
5. Dimitroulas, T., S. N. Nikas, P. Trontzas, and G. D. Kitas. 2013. Biologic therapies and systemic bone loss in rheumatoid arthritis. *Autoimmun. Rev.* 12: 958–966.
6. Pittenger, M. F., A. M. Mackay, S. C. Beck, R. K. Jaiswal, R. Douglas, J. D. Mosca, M. A. Moorman, D. W. Simonetti, S. Craig, and D. R. Marshak. 1999. Multilineage potential of adult human mesenchymal stem cells. *Science* 284: 143–147.
7. Jiang, Y., B. N. Jahagirdar, R. L. Reinhardt, R. E. Schwartz, C. D. Keene, X. R. Ortiz-Gonzalez, M. Reyes, T. Lenvik, T. Lund, M. Blackstad, et al. 2002.

Pluripotency of mesenchymal stem cells derived from adult marrow. *Nature* 418: 41–49.
8. Orbay, H., M. Tobita, and H. Mizuno. 2012. Mesenchymal stem cells isolated from adipose and other tissues: basic biological properties and clinical applications. *Stem Cells Int.* 2012: 461718.
9. English, K. 2013. Mechanisms of mesenchymal stromal cell immunomodulation. *Immunol. Cell Biol.* 91: 19–26.
10. Shi, Y., G. Hu, J. Su, W. Li, Q. Chen, P. Shou, C. Xu, X. Chen, Y. Huang, Z. Zhu, et al. 2010. Mesenchymal stem cells: a new strategy for immunosuppression and tissue repair. *Cell Res.* 20: 510–518.
11. Wang, S., X. Qu, and R. C. Zhao. 2012. Clinical applications of mesenchymal stem cells. *J. Hematol. Oncol.* 5: 19.
12. Wei, X., X. Yang, Z. P. Han, F. F. Qu, L. Shao, and Y. F. Shi. 2013. Mesenchymal stem cells: a new trend for cell therapy. *Acta Pharmacol. Sin.* 34: 747–754.
13. Augello, A., R. Tasso, S. M. Negrini, R. Cancedda, and G. Pennesi. 2007. Cell therapy using allogeneic bone marrow mesenchymal stem cells prevents tissue damage in collagen-induced arthritis. *Arthritis Rheum.* 56: 1175–1186.
14. Chen, M., W. Su, X. Lin, Z. Guo, J. Wang, Q. Zhang, D. Brand, B. Ryffel, J. Huang, Z. Liu, et al. 2013. Adoptive transfer of human gingiva-derived mesenchymal stem cells ameliorates collagen-induced arthritis via suppression of Th1 and Th17 cells and enhancement of regulatory T cell differentiation. *Arthritis Rheum.* 65: 1181–1193.
15. González, M. A., E. Gonzalez-Rey, L. Rico, D. Büscher, and M. Delgado. 2009. Treatment of experimental arthritis by inducing immune tolerance with human adipose-derived mesenchymal stem cells. *Arthritis Rheum.* 60: 1006–1019.
16. Mbalaviele, G., N. Jaiswal, A. Meng, L. Cheng, C. Van Den Bos, and M. Thiede. 1999. Human mesenchymal stem cells promote human osteoclast differentiation from $CD34^+$ bone marrow hematopoietic progenitors. *Endocrinology* 140: 3736–3743.
17. Zhu, H., X. X. Jiang, Z. K. Guo, H. Li, Y. F. Su, H. Y. Yao, X. Y. Wang, X. S. Li, Y. Wu, Y. L. Liu, et al. 2009. Tumor necrosis factor-α alters the modulatory effects of mesenchymal stem cells on osteoclast formation and function. *Stem Cells Dev.* 18: 1473–1484.
18. Oshita, K., K. Yamaoka, N. Udagawa, S. Fukuyo, K. Sonomoto, K. Maeshima, R. Kurihara, K. Nakano, K. Saito, Y. Okada, et al. 2011. Human mesenchymal stem cells inhibit osteoclastogenesis through osteoprotegerin production. *Arthritis Rheum.* 63: 1658–1667.
19. Varin, A., C. Pontikoglou, E. Labat, F. Deschaseaux, and L. Sensebé. 2013. CD200R/CD200 inhibits osteoclastogenesis: new mechanism of osteoclast control by mesenchymal stem cells in human. *PLoS One* 8: e72831.
20. Sung, J. H., H. M. Yang, J. B. Park, G. S. Choi, J. W. Joh, C. H. Kwon, J. M. Chun, S. K. Lee, and S. J. Kim. 2008. Isolation and characterization of mouse mesenchymal stem cells. *Transplant. Proc.* 40: 2649–2654.
21. Tomar, G. B., R. K. Srivastava, N. Gupta, A. P. Barhanpurkar, S. T. Pote, H. M. Jhaveri, G. C. Mishra, and M. R. Wani. 2010. Human gingiva-derived mesenchymal stem cells are superior to bone marrow-derived mesenchymal stem cells for cell therapy in regenerative medicine. *Biochem. Biophys. Res. Commun.* 393: 377–383.
22. Khapli, S. M., L. S. Mangashetti, S. D. Yogesha, and M. R. Wani. 2003. IL-3 acts directly on osteoclast precursors and irreversibly inhibits receptor activator of NF-κB ligand-induced osteoclast differentiation by diverting the cells to macrophage lineage. *J. Immunol.* 171: 142–151.
23. Swarnkar, G., K. Sharan, J. A. Siddiqui, J. S. Mishra, K. Khan, M. P. Khan, V. Gupta, P. Rawat, R. Maurya, A. K. Dwivedi, et al. 2012. A naturally occurring naringenin derivative exerts potent bone anabolic effects by mimicking oestrogen action on osteoblasts. *Br. J. Pharmacol.* 165: 1526–1542.
24. Khan, M. P., A. K. Singh, A. A. Joharapurkar, M. Yadav, S. Shree, H. Kumar, A. Gurjar, J. S. Mishra, M. C. Tiwari, G. K. Nagar, et al. 2015. Pathophysiological mechanism of bone loss in type 2 diabetes involves inverse regulation of osteoblast function by PGC-1α and skeletal muscle atrogenes: AdipoR1 as a potential target for reversing diabetes-induced osteopenia. *Diabetes* 64: 2609–2623.
25. Bouxsein, M. L., S. K. Boyd, B. A. Christiansen, R. E. Guldberg, K. J. Jepsen, and R. Müller. 2010. Guidelines for assessment of bone microstructure in rodents using micro-computed tomography. *J. Bone Miner. Res.* 25: 1468–1486.
26. Yogesha, S. D., S. M. Khapli, R. K. Srivastava, L. S. Mangashetti, S. T. Pote, G. C. Mishra, and M. R. Wani. 2009. IL-3 inhibits TNF-α-induced bone resorption and prevents inflammatory arthritis. *J. Immunol.* 182: 361–370.
27. Lee, S. K., and J. Lorenzo. 2006. Cytokines regulating osteoclast formation and function. *Curr. Opin. Rheumatol.* 18: 411–418.
28. Cho, Y. G., M. L. Cho, S. Y. Min, and H. Y. Kim. 2007. Type II collagen autoimmunity in a mouse model of human rheumatoid arthritis. *Autoimmun. Rev.* 7: 65–70.
29. Morgan, M. E., R. Flierman, L. M. van Duivenvoorde, H. J. Witteveen, W. van Ewijk, J. M. van Laar, R. R. de Vries, and R. E. Toes. 2005. Effective treatment of collagen-induced arthritis by adoptive transfer of $CD25^+$ regulatory T cells. *Arthritis Rheum.* 52: 2212–2221.
30. Kelchtermans, H., L. Geboes, T. Mitera, D. Huskens, G. Leclercq, and P. Matthys. 2009. Activated $CD4^+CD25^+$ regulatory T cells inhibit osteoclastogenesis and collagen-induced arthritis. *Ann. Rheum. Dis.* 68: 744–750.
31. Yanaba, K., Y. Hamaguchi, G. M. Venturi, D. A. Steeber, E. W. St Clair, and T. F. Tedder. 2007. B cell depletion delays collagen-induced arthritis in mice: arthritis induction requires synergy between humoral and cell-mediated immunity. *J. Immunol.* 179: 1369–1380.
32. Yang, M., K. Rui, S. Wang, and L. Lu. 2013. Regulatory B cells in autoimmune diseases. *Cell. Mol. Immunol.* 10: 122–132.
33. Villeneuve, E., and B. Haraoui. 2013. Uncoupling of disease activity and structural damage. Does it matter clinically? *Ann. Rheum. Dis.* 72: 1–2.
34. Choi, J. J., S. A. Yoo, S. J. Park, Y. J. Kang, W. U. Kim, I. H. Oh, and C. S. Cho. 2008. Mesenchymal stem cells overexpressing interleukin-10 attenuate collagen-induced arthritis in mice. *Clin. Exp. Immunol.* 153: 269–276.
35. Djouad, F., V. Fritz, F. Apparailly, P. Louis-Plence, C. Bony, J. Sany, C. Jorgensen, and D. Noël. 2005. Reversal of the immunosuppressive properties of mesenchymal stem cells by tumor necrosis factor α in collagen-induced arthritis. *Arthritis Rheum.* 52: 1595–1603.
36. Park, M. J., H. S. Park, M. L. Cho, H. J. Oh, Y. G. Cho, S. Y. Min, B. H. Chung, J. W. Lee, H. Y. Kim, and S. G. Cho. 2011. Transforming growth factor β-transduced mesenchymal stem cells ameliorate experimental autoimmune arthritis through reciprocal regulation of Treg/Th17 cells and osteoclastogenesis. *Arthritis Rheum.* 63: 1668–1680.
37. Schurgers, E., H. Kelchtermans, T. Mitera, L. Geboes, and P. Matthys. 2010. Discrepancy between the in vitro and in vivo effects of murine mesenchymal stem cells on T-cell proliferation and collagen-induced arthritis. *Arthritis Res. Ther.* 12: R31.
38. Zhou, B., J. Yuan, Y. Zhou, M. Ghawji, Jr., Y. P. Deng, A. J. Lee, A. J. Lee, U. Nair, A. H. Kang, D. D. Brand, and T. J. Yoo. 2011. Administering human adipose-derived mesenchymal stem cells to prevent and treat experimental arthritis. *Clin. Immunol.* 141: 328–337.
39. Chen, H., X. Zhou, H. Fujita, M. Onozuka, and K. Y. Kubo. 2013. Age-related changes in trabecular and cortical bone microstructure. *Int. J. Endocrinol.* 2013: 213234.
40. Tanaka, K., M. Hashizume, M. Mihara, H. Yoshida, M. Suzuki, and Y. Matsumoto. 2014. Anti-interleukin-6 receptor antibody prevents systemic bone mass loss via reducing the number of osteoclast precursors in bone marrow in a collagen-induced arthritis model. *Clin. Exp. Immunol.* 175: 172–180.
41. Walsh, N. C., S. Reinwald, C. A. Manning, K. W. Condon, K. Iwata, D. B. Burr, and E. M. Gravallese. 2009. Osteoblast function is compromised at sites of focal bone erosion in inflammatory arthritis. *J. Bone Miner. Res.* 24: 1572–1585.
42. Lacey, D. C., P. J. Simmons, S. E. Graves, and J. A. Hamilton. 2009. Proinflammatory cytokines inhibit osteogenic differentiation from stem cells: implications for bone repair during inflammation. *Osteoarthritis Cartilage* 17: 735–742.
43. Sakaguchi, S., T. Yamaguchi, T. Nomura, and M. Ono. 2008. Regulatory T cells and immune tolerance. *Cell* 133: 775–787.
44. Zaiss, M. M., B. Frey, A. Hess, J. Zwerina, J. Luther, F. Nimmerjahn, K. Engelke, G. Kollias, T. Hünig, G. Schett, and J. P. David. 2010. Regulatory T cells protect from local and systemic bone destruction in arthritis. *J. Immunol.* 184: 7238–7246.
45. Matsushita, T., K. Yanaba, J. D. Bouaziz, M. Fujimoto, and T. F. Tedder. 2008. Regulatory B cells inhibit EAE initiation in mice while other B cells promote disease progression. *J. Clin. Invest.* 118: 3420–3430.
46. Carter, N. A., R. Vasconcellos, E. C. Rosser, C. Tulone, A. Muñoz-Suano, M. Kamanaka, M. R. Ehrenstein, R. A. Flavell, and C. Mauri. 2011. Mice lacking endogenous IL-10-producing regulatory B cells develop exacerbated disease and present with an increased frequency of Th1/Th17 but a decrease in regulatory T cells. *J. Immunol.* 186: 5569–5579.
47. Guo, Y., K. H. Chan, W. H. Lai, C. W. Siu, S. C. Kwan, H. F. Tse, P. Wing-Lok Ho, and J. Wing-Man Ho. 2013. Human mesenchymal stem cells upregulate $CD1dCD5^+$ regulatory B cells in experimental autoimmune encephalomyelitis. *Neuroimmunomodulation* 20: 294–303.